Title
Universal quasiparticle decoherence in hole- and electron-doped high-Tc cuprates

Authors
Pan, Z-H
Richard, P
Fedorov, AV
et al.

Publication Date
2006-10-16

Peer reviewed

Universal quasiparticle decoherence in hole- and electron-doped high-T_c cuprates

Z.-H. Pan,[1] P. Richard,[1] A.V. Fedorov,[2] T. Kondo,[3] T. Takeuchi,[3]
S.L. Li,[4] Pengcheng Dai,[4,5] G.D. Gu,[6] W. Ku,[6] Z. Wang,[1] and H. Ding[1]
(1) Department of Physics, Boston College, Chestnut Hill, MA 02467
(2) Advanced Light Source, Lawrence Berkeley National Laboratory, Berkeley, CA 94720
(3) Research center for advanced waste and emission management, Nagoya University, Japan
(4) Department of Physics and Astronomy, University of Tennessee, Knoxville, TN 37996
(5) Neutron Scattering Sciences Division, Oak Ridge National Laboratory, Oak Ridge, TN 37831
(6) Condensed Matter and Materials Science Department,
Brookhaven National Laboratory, Upton, New York 11973

We use angle-resolved photoemission to unravel the quasiparticle decoherence process in the high-T_c cuprates. The coherent band is highly renormalized, and the incoherent part manifests itself as a nearly vertical "dive" in the E-k intensity plot that approaches the bare band bottom. We find that the coherence-incoherence crossover energies in the hole- and electron-doped cuprates are quite different, but scale to their corresponding bare bandwidth. This rules out antiferromagnetic fluctuations as the main source for decoherence. We also observe the coherent band bottom at the zone center, whose intensity is strongly suppressed by the decoherence process. Consequently, the coherent band dispersion for both hole- and electron-doped cuprates is obtained, and is qualitatively consistent with the framework of Gutzwiller projection.

Understanding the electronic structure and properties in strongly correlated systems, in particular in the high–T_c cuprates, has been a main focus in condensed matter physics over the past two decades. Unlike in simple metals and insulators, the presence of strong correlation makes the predictions of band calculations such as the LDA unreliable. Much of the theoretical understanding, based upon studies of Hubbard-like models, is the existence of strongly renormalized coherent quasiparticle excitations of a much reduced bandwidth *à la* Brinkman-Rice [1] and Gutzwiller wavefunctions [2], and large incoherent background of the Mott-Hubbard [3] type that extends to the bare band edge [4]. Both features have been ubiquitously observed in the cuprates, yet the precise description of the one-particle spectral function over the range of bare bandwidth provided by LDA remained incomplete due to the complexity of this many-body problem. The correlation-induced thermodynamic mass renormalization in the cuprate is ~ 3, which can be directly extracted from the renormalized Fermi velocity determined from angle-resolved photoelectron spectroscopy (ARPES) in the prototype $Bi_2Sr_2CaCu_2O_{8+\delta}$. Many ARPES measurements have been performed to determine the band dispersion in the high-T_c cuprates. Remarkably, the band dispersion for the quasiparticle excitations can only be traced up to ~ 350 meV, above which the band seems to disappear and the anticipated band bottom at the Γ (0,0) point has not been identified [5]. A recent ARPES on the undoped cuprate $Ca_2CuO_2Cl_2$ also found that the renormalized band is truncated around 350 meV, and the incoherent part at high energy seems to follow the bare band dispersion predicted by LDA [6]. It was suggested that the cause of this truncation is the antiferromagnetic fluctuations, with a characteristic energy scale of $2J$, where $J \sim 120 - 160$ meV is the superexchange coupling of the Cu-O square lattice.

In this Letter, we report a systematic APRES study on the complete band dispersion of various cuprates, including hole-doped $Pb_xBi_{2-x}Sr_2CuO_{6+\delta}$ and electron-doped $Pr_{1-x}LaCe_xCuO_4$. The most important of our findings is that the truncation energy scale of the coherence-incoherence crossover is *not* fixed around 350 meV, or $\sim 2J$, instead it is determined by and scales with the bare bandwidth. In the electron-doped cuprates, this crossover along $\Gamma - X$ occurs around ~ 600 meV, much larger than the value (350 meV) in the hole-doped ones. At binding energies above the crossover, the incoherent part of the spectrum takes the form of a nearly vertical dispersion around a fixed crystal momentum k, and approaches the bare band bottom predicted by LDA. In addition, we observe for the first time the bottom of the renormalized band whose intensity is strongly suppressed. The complete determination of the coherent part of the occupied Cu3$d_{x^2-y^2}$ band enables us to provide the tight-binding parameters and compare to the more realistic quasiparticle dispersion calculated from models with strong local correlation. We find that the renormalized dispersion obtained from the Gutzwiller projected wavefunction approach to the $t - J$ like models is a promising candidate for the observed low energy quasiparticle band.

High quality single crystals of cuprates $Pb_xBi_{2-x}Sr_2CuO_{6+\delta}$ (Pb-Bi2201), $Bi_2Sr_2CaCu_2O_{8+\delta}$ (Bi2212), and $Pr_{1-x}LaCe_xCuO_4$ (PLCCO) were prepared by the the traveling solvent floating zone method, and some were annealed subsequently. ARPES experiments were performed at the Synchrotron Radiation Center, WI, and the Advanced Light Source, CA. High-resolution undulator beamlines and Scienta analyzers with a capability of multi-angle detection have been used. The energies of photons were carefully chosen in order to enhance certain spectral features. The energy resolution is $\sim$ 10 - 30 meV, and the momentum resolution ~ 0.02 Å^{-1}. All the samples were cleaved and

measured *in situ* in a vacuum better than 8×10^{-11} *Torr* at low temperatures (14 - 40 K) on a flat (001) surface, and all the spectra shown below have been reproduced on multiple samples.

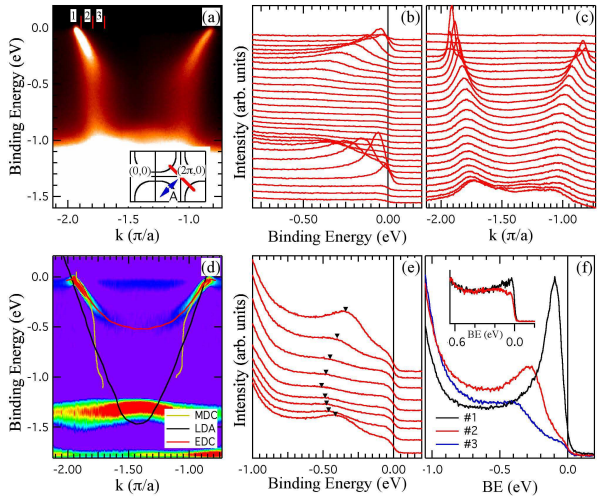

FIG. 1: Dispersion of coherent and incoherent bands along $\Gamma-X$ in Pb-Bi2201 measured at 20K using 57-eV *s*-polarized photons. (a) - (d) Plots of E-k intensity, EDCs, MDCs, and the second derivative intensity, respectively. The inset in panel (a) displays the measurement locations in BZ. In panel (d), three extra lines of dispersion extracted from EDCs (red), MDCs (yellow), and LDA calculation (black) are also superimposed for the comparison purpose. (e) Magnified plot for EDCs near Γ. (f) Comparison of three EDCs at the k-locations labeled as #1 to #3 in Fig. 1a. The inset shows two EDCs of Bi2212 at the similar k-locations as #1 and #2, but using p-polarized photons.

We start with a set of spectra along $\Gamma-X$ on a hole-doped $Pb_xBi_{2-x}Sr_2CuO_{6+\delta}$ (overdoped $T_c\sim7$K), as shown in Fig. 1. The reason we choose this material is that the Pb substitutions remove the superlattice modulation in Bi-O plane, which often complicates ARPES spectra [7]. The spectra were taken along $\Gamma-X$ in the second Brillouin zone (BZ) using 57-eV *s*-polarized ($\vec{A}\parallel\Gamma X$) photons to enhance various features at high binding energy (>350 meV). In Fig. 1a, one can easily follow the dispersive band at low energy (<350 meV). This band is the well-know Zhang-Rice singlet [8], with the predominant Cu3$d_{x^2-y^2}$-O2$p_{x,y}$ antibonding orbital. While the Fermi vector k_F is almost the same as the one predicted by LDA, as shown in Fig. 1d, its dispersion velocity v_k (~2.1 eVÅ) is much smaller than the LDA value (~5.2 eVÅ) [9], consistent with previous ARPES results [7, 10, 11]. Note that the Fermi velocity v_F (~1.6 eVÅ) at k_F is even smaller due to a further renormalization by the observed nodal kink at ~70 meV [12, 13], which is difficult to visualize at the large energy scale in Fig. 1. At higher binding energy (>350 meV), the spectrum becomes ill-defined. While the intensity plot (Fig. 1a) seems to indicate that the spectra abruptly "dive" almost vertically from 350 meV to at least 1 eV, this diving behavior does not expressed itself as a peak in the energy distribution curves (EDCs) (Fig. 1b). Instead, an enhancement in the EDC background is observed at the k-location of the dive around ($\pi/4$, $\pi/4$) and equivalent k points in other BZs, as shown in Fig. 1f where the EDC at the dive location (# 2, as marked in Fig. 1a) has a higher background than its neighboring EDCs (*e.g.*, # 1 and # 3). The diving behavior is reflected more clearly in the momentum distribution curves (MDCs), as shown in Figs. 1d where the MDCs seem to maintain their peak shape. Since the dive completely loses the peak (or pole) structure in energy, strictly it is no longer a band. Nevertheless, it is likely the incoherent part of the Cu3$d_{x^2-y^2}$-O2$p_{x,y}$ (or ZRS) spectrum, since it maintains the $d_{x^2-y^2}$ symmetry. We have verified this symmetry, as shown in the inset of Fig. 1f, where both the coherent band and the dive are suppressed by p-polarized light ($\vec{A}\perp\Gamma X$). This is due to a well-known ARPES selection rule [14]. In addition, we have also observed that the intensity ratio between these two features is roughly a constant when we change s and p polarization components, supporting that the dive is the incoherent part of the band.

So far we have shown that the coherent ZRS band disperses to a certain energy (~350 meV) and then abruptly switches to the incoherent part at the higher energies. However, if we take a closer look at the EDCs in the vicinity of Γ, we observe the smooth continuation of the coherent band, which reaches the bottom around 0.5 eV at Γ, as shown in Fig. 1e. This is the long-sought-after renormalized band bottom, and the reason we can observe it for the first time is due to several combined factors such as the superlattice free sample, a proper photon energy, and the second BZ, all of which enhance the intensity of the high-energy features. We note that the coherent band starts to lose its intensity at the same energy where the incoherent diving pattern begins to form, indicating a weight transfer between the coherent and incoherent parts. The bottom of the coherent band can be also visualized, as shown in Fig. 1d, from the second derivative of the intensity with respect to energy which enhances broad horizontal features. In Fig. 1d, we compare the dispersion of the coherent band with the calculated one from LDA, along with the dispersion extracted from MDCs. It is clear that the coherent band, with a well-defined parabolic shape, is highly renormalized, and the vertical feature is likely the incoherent part, which approaches the bottom of the bare band.

We have observed very similar behaviors of the coherence-incoherence crossover in the bilayer system $Bi_2Sr_2CaCu_2O_{8+\delta}$, except the superlattice in this material makes it difficult to observe the bottom formation of the coherent band at Γ. Like in Pb-Bi2201, the incoherent part in Bi2212 deviates from the coherent part around 350 meV, and approaches almost vertically the bare band bottom around 1.5 eV. Since the 350 meV energy scale of the coherence-incoherence crossover has been attributed to the antiferromagnetic fluctuations whose characteristic energy scale $2J$ has a similar value [6], it is natural to

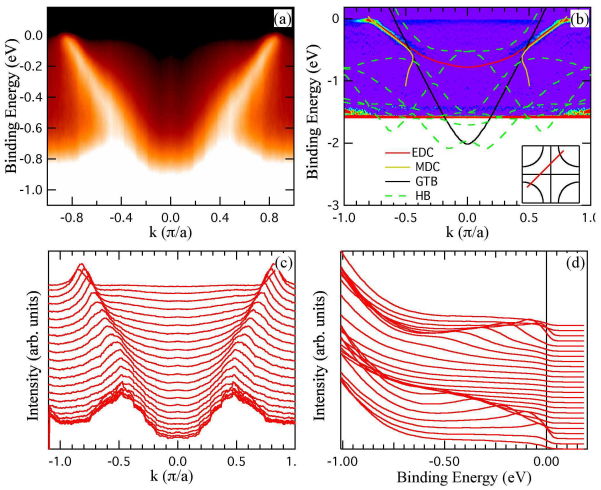

FIG. 2: Dispersion of the coherent and incoherent bands near $\Gamma - X$ in PLCCO measured at 40 K using 22-eV photons. (a) - (d) Plots of E-k intensity, second derivative intensity, EDCs, and MDCs, respectively. The inset in panel (b) displays the measurement locations in BZ. The superimposed curves in panel (b) are the extracted EDC positions (red), fitted MDC positions (yellow), non-hybridized LDA band (solid black), and hybridized LDA bands (dashed green).

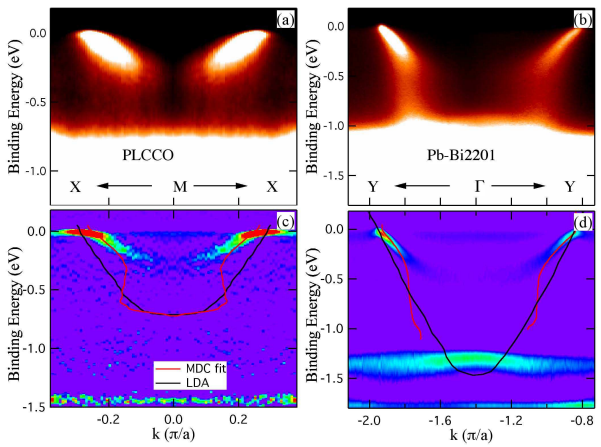

FIG. 3: Comparison of band dispersion between $M - X$ in PLCCO using 22-eV photons and $\Gamma - X$ in Pb-Bi2201 using 57-eV photons. (a) - (b) E-k intensity plots for $M - X$ in PLCCO and $\Gamma - X$ in Bi2201, respectively. (c) - (d) Corresponding second derivative plots for panels (a) and (b), respectively. MDC dispersion (red lines) and bare band from LDA (black lines) are superimposed to the plots in panels (c) and (d).

check if a similar coherence-incoherence crossover exists in the electron-doped cuprates. We have searched for this crossover on various electron-doped cuprates, and the main results are presented in the following two figures.

We first show, in Fig. 2, the dispersion of the electron-doped cuprate $Pr_{0.88}LaCe_{0.12}CuO_4$ ($T_c \sim 23$ K) near $\Gamma - X$ using 22-eV p-polarized photons. Since the band intensity exactly along $\Gamma - X$ is highly suppressed due to the selection rule mentioned above, we choose to display the dispersion along the parallel direction slightly away from the $\Gamma - X$ direction, as indicted in the inset of Fig. 2b. A quick examination of the plots of Fig. 2 reveals a major difference to the hole-doped materials: the coherent band in PLCCO extends to a much higher binding energy. The separation of the incoherent part occurs around 0.6-0.7 eV, which also forms a diving pattern at higher binding energy, as seen in both the intensity plot in Fig. 2a and the MDCs plot in Fig. 2c. We note that the diving pattern appears to be shorter than the one in the hole-doped cuprates. We believe that this is due to the hybridization between the Cu3$d_{x^2-y^2}$ band and some other bands, as predicted by LDA calculations [15] and shown in Fig. 2b (dashed green curves). The bare Cu3$d_{x^2-y^2}$ band, while not mixing with those bands, reaches the bottom around 2.1 eV, as indicted in Fig. 2b (solid black curves) [16]. In comparison, the coherent part has its band bottom around 0.8 eV, indicating a mass renormalization of 2.5, similar as in the hole-doped case.

The different energy scale of the coherence-incoherence crossover in the electron-doped cuprates, as observed in PLCCO and confirmed in other electron-doped materials, such as $Pr_{2-x}Ce_xCuO_4$ and $Nd_{2-x}Ce_xCuO_4$, argues strongly against the antiferromagnetic scenario. Instead, the same mass renormalization ratio in both cases suggests that this energy scale may be related to the bare bandwidth. This is also true in the electron-doped material along another high-symmetry direction, $M - X$, as can be seen in Fig. 3. It is well known that the van-Hove saddle point shifts to a much higher binding energy ($\sim$ 0.4 eV) in the electron-doped cuprates [17, 18]. Over the wide energy range, the Cu3$d_{x^2-y^2}$ band dispersion along $M - X$ in PLCCO has many similarities to the band along $\Gamma - X$ in Bi2201, as shown in Fig. 3. The coherent part along $M - X$ in PLCCO, while being quite broad due to the possible stronger interactions near the antinode, extends to an energy scale ($\sim$ 0.25 eV) when the incoherent part takes a dive. The bottom of the coherent part at M is estimated to be $\sim$ 0.3 eV, and the bare band position at M is calculated by LDA to be $\sim$ 0.7 eV. For comparison, we draw both intensity plot and second derivative plot of Pb-Bi2201 in the left panels of Fig. 3 in a slightly reduced energy scale. We also notice that there is a small kink at $\sim$ 70 meV along $M - X$ in PLCCO, which resembles the well-know and much-debated nodal kink in the holed-doped cuprates [12, 13]. We caution that the origin of the antinodal kink in PLCCO may not be the same as the antinodal one in the hole-doped case, and call for more systematic studies.

We have measured band dispersion along many directions in the BZ for various hole- and electron-doped cuprates. In Fig. 4, we summarize our main results as a comparison between the coherent band dispersion and the bare band dispersion predicted by LDA along several high-symmetry directions, for both Pb-Bi2201 ($T_c \sim 7$

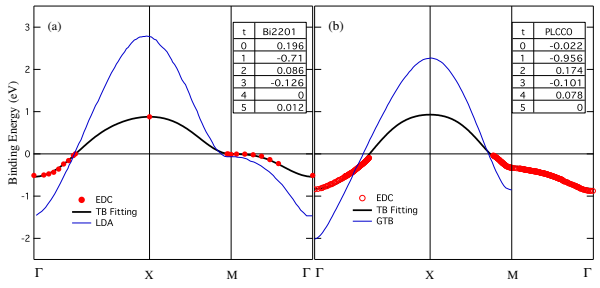

FIG. 4: Summary of coherent band dispersion along three principle directions (Γ-X, X-M, and M-Γ) for hole- and electron-doped cuprates. (a) - (b) Measured coherent band position (red dots), tight-binding fit (black solid line), and LDA band dispersion (blue dashed line) in Pb-Bi2201 and PLCCO, respectively. The inserted tables are the obtained fitting parameters.

K) and PLCCO ($T_c \sim 23$ K) samples. We also use the effective tight-binding band to fit the coherent dispersion, using the standard formula as in previous work [5]. Since ARPES only measures the occupied side, we adapt the previous method [5] by choosing the unoccupied band top at X (π, π) in such a way that it maintains the same band renormalization ratio (~ 2.5) as the occupied side. We use the six free parameters (t_0 to t_5) with t_0 being the chemical potential, t_1 the nearest neighboring hopping term, and t_2 to t_5 the higher order hopping terms. The numeric values of these parameters are also listed in Fig. 4. The large difference of t_0 (~ 0.4 eV) between the two systems indicates a large chemical shift from the hole doped side to the electron doped side, which is likely the main cause of the downshift of (~ 0.4 eV) of the van Hove singularity in the electron-doped cuprates.

In summary, we have determined by ARPES the complete low energy quasiparticle dispersion and elucidated its unusual evolution to the high energy incoherent background in both hole- and electron-doped cuprates. The reduction of the bandwidth from its bare value is most likely the result of strong local correlations that frustrate the kinetic energy. This is overall consistent with the Gutzwiller projected wavefunction approach to simple models of doped Mott insulators [19]. Detailed comparisons would require measurement of the doping dependence of the renormalized bandwidth, which is more difficult to determine due to the doping dependent shift of the chemical potential. More systematic studies are needed to clarify this issue. Most surprisingly, we find that the energy scale associated with the coherence-incoherence crossover is determined by a fraction of the bare band bottom energy and is in general different from the antiferromagnetic exchange energy $2J$, ruling out the latter as the main cause of quasiparticle decoherence at *high* binding energies. Moreover, it appears more universal that the incoherent spectrum beyond the decoherence energy takes a vertical dive with a nearly fixed $k \sim (\pi/4, \pi/4)$, approaching the bottom of the bare band in what seems to be the "cheapest" way for the renormalized quasiparticles to return to their bare form. The origin of these unexpected behaviors is largely unknown and demands more understanding of the interplay between the coherent quasiparticle and collective excitations and the dominant incoherent processes in the spectral function, which has been one of the central challenges in the physics of strong correlations.

We thank P.W. Anderson, D.H. Lee, M.R. Norman, F.C. Zhang for valuable discussions and suggestions. This work is supported by NSF DMR-0353108, DOE DE-FG02-99ER45747, DE-FG02-05ER46202, and DE-AC02-98CH10886. ZHP is also supported by ALS Doctoral Fellowship in Residence. This work is based upon research conducted at the Synchrotron Radiation Center supported by NSF DMR-0084402, and at the Advanced Light Source supported by DOE DE-AC03-76SF00098. ORNL is supported by DOE under contract No. DE-AC05-00OR22725 with UT/Battelle, LLC.

Note added: During the preparation of this manuscript, we became aware of three preprints reporting independently ARPES results of band dispersion over a large energy scale on the hole-doped cuprates [20, 21, 22].

[1] W. Brinkman and T.M. Rice, Phys. Rev. B **2**, 4302 (1970).
[2] M.C. Gutzwiller, Phys. Rev. Lett. **10**, 159 (1963).
[3] J. Hubbard, Proc. R. Soc. London A **276**, 238 (1963); **277**, 237 (1964);**296**, 82 (1967).
[4] Z. Wang, Y.K. Bang, and G. Kotliar, Phys. Rev. Lett. **67**, 2733 (1991).
[5] M.R. Norman, M. Randeria, H. Ding, and J.C. Campuzano, Phys. Rev. B **52**, 615 (1995).
[6] F. Ronning *et al.*, Phys. Rev. B **71**, 094518 (2005).
[7] H. Ding *et al.*, Phys. Rev. Lett. **76**, 1533 (1996).
[8] F.C. Zhang and T.M. Rice, Phys. Rev. B **37**, 3759 (1988).
[9] M.S. Hybertsen and L.F. Mattheiss, Phys. Rev. Lett. **60**, 1661 (1988); H. Krakauer and W.E. Pickett, Phys. Rev. Lett. **60**, 1665 (1988).
[10] D.S. Dessau *et al.*, Phys. Rev. Lett. **71**, 2781 (1993).
[11] T. Valla *et al.*, Phys. Rev. Lett. **85**, 828 (2000).
[12] T. Valla *et al.*, Science **285**, 2110 (1999).
[13] A. Lanzara *et al.*, Nature **412**, 510 (2001).
[14] M.R. Norman *et al.*, Phys. Rev. B **52**, 15107 (1995).
[15] S. Massida *et al.*, Physica C **157**, 571 (1989).
[16] V.A. Gavrichkov *et al.*, Phys. Rev. B **72**, 165104 (2005).
[17] D.M. King *et al.*, Phys. Rev. Lett. **70**, 3159 (1993).
[18] T. Sato *et al.*, Science **291**, 1517 (2001).
[19] P.W. Anderson *et al.*, J Phys. Condens. Matter **16** R755, (2004).
[20] J. Graf *et al.*, *cond-mat*/0607319.
[21] B.P. Xie *et al.*, *cond-mat*/0607450.
[22] T. Valla *et al.*, *cond-mat*/0610249.